Journal of Magnetism and Magnetic Materials ∎ (∎∎∎∎) ∎∎∎–∎∎∎

Contents lists available at ScienceDirect

Journal of Magnetism and Magnetic Materials

journal homepage: www.elsevier.com/locate/jmmm

A wide-frequency range AC magnetometer to measure the specific absorption rate in nanoparticles for magnetic hyperthermia

E. Garaio [a,*], J.M. Collantes [a], J.A. Garcia [b], F. Plazaola [a], S. Mornet [c], F. Couillaud [d], O. Sandre [e,*]

[a] Elektrizitatea eta Elektronika Saila, UPV/EHU, P.K. 644, Bilbao, Spain
[b] Fisika Aplikatua II Saila, UPV/EHU, P.K. 644, Bilbao, Spain
[c] Institut de Chimie de la Matière Condensée de Bordeaux, UPR 9048 CNRS / Université de Bordeaux, Bordeaux, France
[d] Résonance Magnétique des Systèmes Biologiques, UMR 5536 CNRS / Université de Bordeaux, Bordeaux, France
[e] Laboratoire de Chimie des Polymères Organiques, UMR 5629 CNRS / Université de Bordeaux, Bordeaux, France

ARTICLE INFO

Keywords:
Specific absorption rate
Maghemite nanoparticle
Magnetic hyperthermia
AC magnetometer

ABSTRACT

Measurement of specific absorption rate (*SAR*) of magnetic nanoparticles is crucial to assert their potential for magnetic hyperthermia. To perform this task, calorimetric methods are widely used. However, those methods are not very accurate and are difficult to standardize. In this paper, we present AC magnetometry results performed with a lab-made magnetometer that is able to obtain dynamic hysteresis-loops in the AC magnetic field frequency range from 50 kHz to 1 MHz and intensities up to 24 kA m^{-1}. In this work, *SAR* values of maghemite nanoparticles dispersed in water are measured by AC magnetometry. The so-obtained values are compared with the *SAR* measured by calorimetric methods. Both measurements, by calorimetry and magnetometry, are in good agreement. Therefore, the presented AC magnetometer is a suitable way to obtain *SAR* values of magnetic nanoparticles.

1. Introduction

Hyperthermia based therapies are medical practices that consist of rising the temperature of living tissue above the physiological values. They are useful for cancer treatment (i) to damage and kill cancer cells (thermo-ablation), (ii) to change their sensitivity to radiation or drugs (thermo-sensitization) or to (iii) induce local drug release from thermo-sensitive vehicles. As hyperthermia could be performed locally, therapy essentially affects the targeted tumor avoiding damage to surrounding tissues and limiting systemic effects [1,2]. Photons (Laser), microwaves, radio-frequency or focused ultrasound are energy sources used for local hyperthermia. Magnetic nanoparticles that release heat while activated in an alternating magnetic field have also been proposed to induce tumor hyperthermia [3,4]. Such magnetically activated nanoparticles have been shown to enhance efficacy of radiotherapy and chemotherapy against cancer [5,6]. This approach passed a phase II clinical trial in conjunction with conventional radiotherapy [7] and is authorized for cancer treatment since 2011.

To further assess the potential of magnetic nanoparticles for magnetic hyperthermia, accurate measurement of their heat dissipation rate is necessary. In other words, their specific absorption rate (*SAR*), which corresponds to the absorbed energy per unit of mass of nanoparticle, has to be determined. This parameter is quite dependent on magnetic field frequency and intensity as well as on nanoparticle size, shape, material, agglomeration rate and dispersion media [8–10].

At present, mainly calorimetric methods [8,10–12] are used to measure *SAR* values of magnetic nanoparticles. For nanoparticles dispersed in a fluid medium, the specific absorption rate is obtained experimentally by the following formula [13]:

$$SAR = \frac{m_d C_{p,d}}{m_{NP}} \left| \frac{dT}{dt} \right|_{t=0} \quad (1)$$

where m_d and $C_{p,d}$ are the mass and heat capacity of the dispersion medium respectively while m_{NP} is the mass of nanoparticles. However, there are many factors that affect the accuracy of calorimetric methods [13,14]. For samples with high absorption power, fast heating causes large temperature gradients into the sample and thus, the recorded *SAR* can be very dependent on temperature sensor positioning [13]. The method and time interval used to determine initial temperature slope in Eq. (1) also adds uncertainties [13]. In addition, thermal losses also cause underestimating the *SAR* value, thus properly designed adiabatic conditions for the experiment are needed [15]. Therefore the volume and geometry of the sample are important to specify for reasons related to the homogeneity of the applied magnetic field and to the surface-to-volume ratio, determining the heat transfers.

* Corresponding authors. Tel.: +34 696725466.
E-mail addresses: eneko.garayo@ehu.es (E. Garaio), olivier.sandre@enscbp.fr (O. Sandre).

0304-8853/$ - see front matter © 2013 Elsevier B.V. All rights reserved.
http://dx.doi.org/10.1016/j.jmmm.2013.11.021

SAR measurements by calorimetry are indeed based on the measurement of the maximum slope of the temperature increase, Eq. (1), but the extension of the linear regime is always limited (except for ideal adiabatic conditions) by a plateau value ΔT_{max}, after a duration that increases with the sample volume. This maximum temperature increment that can be reached by magnetic field hyperthermia (*MFH*) directly depends on the surface area of the sample, as demonstrated by the square dependence with diameter on magnetic droplets in a microfluidic circuit [16].

In order to find a more accurate method to obtain the *SAR* of magnetic nanoparticles, different ways are proposed in the literature. Ahrentorp et al. [17] obtained *SAR* values by combining AC magnetic susceptibility and static magnetization curves. Also, methods based on Faraday's law of induction to obtain the dynamic magnetization, $M(t)$, are proposed. Cobos et al. [18] measured the power dissipated by the nanoparticles through the determination of their in-quadrature magnetic moment. In other works, however, the *SAR* was obtained directly from AC hysteresis loops area in a small [19] and large [20–23] applied magnetic field regime. In these works based on Faraday's induction law, the applied magnetic field frequency was always below 130 kHz.

In this paper, we present an AC magnetometer to measure dynamic hysteresis cycles of magnetic nanoparticle dispersions, which extends the range of measurement up to 1 MHz. This gives valuable information on their dynamic magnetic behavior. Furthermore, the *SAR* value can be directly obtained from the area of the hysteresis cycles. The device is based on Faraday's induction law and works in the frequency range 50 kHz to 1 MHz. To calibrate the system at high frequencies (above 250 kHz), a personal computer (PC) performs a Fourier analysis of the signal induced by the sample. In the present work, *SAR* values of maghemite (γ-Fe_2O_3) nanoparticles dispersed in water are measured and compared to the values obtained by calorimetric methods.

2. Experimental

2.1. Magnetic nanoparticles

The magnetic nanoparticles are synthesized by the aqueous alkaline co-precipitation route of Fe^{2+} and Fe^{3+} salts, also called Massart's synthesis [24]. The resulting nanoparticles of magnetite (Fe_3O_4) are oxidized by iron nitrate into the pure Fe^{+III} isomorphous maghemite phase [25]. Compared to other syntheses at high temperature in non-aqueous media, the co-precipitation route has the advantage of providing large quantity (hundreds of g) but the drawback of a very large size-dispersity (typically from 5 to 20 nm). Therefore a size-grading method based on successive phase separation by adding electrolyte in excess was applied [26]. Briefly, after synthesis the maghemite nanoparticles are dispersed in water in a nitric acidic medium (pH ~ 2). Their dipolar attractions (Van der Waals and magnetic) are counterbalanced by electrostatic (double-layer) repulsion arising from the cationic charges at their surface. The addition of an excess of HNO_3 (pH ~ 0.7–0.8) causes the screening of the charges and the destabilization of the suspension into two phases, respectively concentrated (liquid-like) and diluted (gas-like). After magnetic sedimentation, the concentrated phase (C) is separated from the dilute supernatant (S) that is enriched in nanoparticles of smaller diameters (on the contrary, the C phase is enriched with the larger diameters). The process is repeated to isolate different fractions with much narrower size distribution than the initial suspension. In this work we need nanoparticles of the largest possible diameters to achieve a high *SAR* value, thus we study the $C_1C_2C_3$ fraction (after three separation steps). The exact procedure of phase separation and washing steps is detailed in the supporting information of several references [27,28].

The weight concentration of this $C_1C_2C_3$ fraction is $c_0 = 99\ g\ L^{-1} = 9.9 \times 10^4\ g\ m^{-3}$ as measured by magnetometry (Fig. 1) and UV–vis spectroscopy (Fig. 2). It was diluted 3 times ($c = 33\ g\ L^{-1}$) to perform both the calorimetry and dynamic hysteresis measurements. The accurate determination of concentration of iron oxide in the suspension is a pre-requisite for a proper *SAR* measurement. Regarding colloidal stability, the hydrodynamic diameter of the $C_1C_2C_3$ fraction diluted 400 times in HNO_3 at pH ~2 is 32 ± 0.8 nm (from 5 successive measurements by dynamic light scattering at 90 °C with a NanoZS90 instrument, Malvern, UK), with a low polydispersity index (PDI = 0.137). These nanoparticles are thus perfectly stable, as expected from the electrostatic repulsions created by their positive surfaces charges in acidic medium. It is in this diluted state that the iron oxide concentration was checked by a non-destructive method consisting in recording the whole UV–vis absorption spectrum from 240 to 800 nm and comparing it to a calibration curve derived from standards [29].

2.2. Description of the AC magnetometer

The AC magnetic field is generated by an air-coil connected in parallel with a resonant circuit fed by a linear power amplifier [30]. The system that acquires the dynamic magnetization of the sample, $M(t)$, consists of tree pickup coils (see Fig. 3). Inside the air-coil, two concentric and oppositely wounded pickup coils connected in series are placed, one on top of the other (coils 1 and 2 in Fig. 3). The upper coil surrounds the sample holder located in the center of the coil and the lower one, called compensation coil, is located in such a way that without any sample in the sample-holder, the induced voltage is minimal. The third pickup coil, placed outside the air-coil, measures the applied magnetic field intensity and phase (coil 3 in Fig. 3). It has been checked that the signal induced in this coil is exactly in phase with the magnetic field intensity applied to the sample for all frequencies. The magnetization $M(t)$ is obtained by

$$V(t) = \xi \cdot f \cdot M(t) \tag{2}$$

where f is the magnetic field frequency and ξ a coupling constant calculated numerically from the setup geometry. The signal $V(t)$ induced by the sample into the pick-up coils is recorded by a data acquisition system and sent to a PC.

Temperature of the sample is recorded by a fiber optic thermometer insensitive to RF magnetic fields with a narrow tip of 0.4 mm (Opsens, Québec, QC, Canada). In order to avoid thermal dilatation and minimize heat flow out of the sample, the sample-holder is made of ceramic material.

The sample holder is cylindrical with a volume of 1.5 mL and aspect ratio L/d of 3 (this parameter is important to specify both for the surface area and the demagnetization factor of the magnetized sample). Due to the lack of perfect symmetry of the two pick-up coils connected in series, a non-zero voltage is recorded even when there is no magnetic sample. To calibrate it, the induced voltage magnitude and phase in the absence of the sample are stored. Then, these values are used to vectorially compensate the signal measured when the sample is present. As it can be appreciated on the AC hysteresis loops present in Fig. 4, the magnetization curves at different applied magnetic field intensities do not cross each other, which confirms the correct compensation.

At high frequencies (above 250 kHz), the contribution of higher order harmonics generated by the power amplifier that feeds the

Please cite this article as: E. Garaio, et al., Journal of Magnetism and Magnetic Materials (2013), http://dx.doi.org/10.1016/j.jmmm.2013.11.021

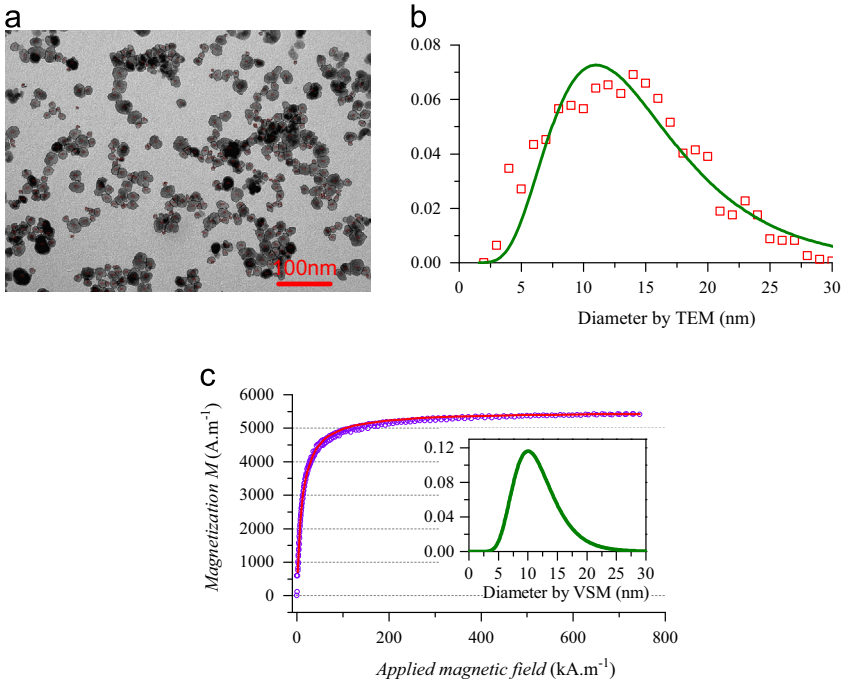

Fig. 1. (a) TEM image of the size-sorted fraction $C_1C_2C_3$ (scale bar length is 100 nm). The image is processed with ImageJ with a threshold and a watershed filter in order to detect the border lines of the nanoparticles and enable an automatic counting; (b) histogram built by processing 5 images with a statistics on $N \sim 1600$ nanoparticles; the solid line is a Log-normal distribution of median $d_0^{TEM} = 13.5$ nm and standard width $\sigma^{TEM} = 0.45$; (c) magnetization curve obtained on a lab-made vibrating sample magnetometry (VSM). The curve is fitted by the Langevin law of superparamagnetism convolved with a Log-normal distribution of median $d_0^{VSM} = 11.2$ nm and standard width $\sigma^{VSM} = 0.325$ (see distribution curve in inset). The respective number-average diameters are $\langle d \rangle^{TEM} = 16$ nm and $\langle d \rangle^{VSM} = 12$ nm, the gap between the two measurements being ascribed to a magnetically disordered layer around the maghemite nanoparticles. The saturation value at large field being $M_{sat} = 5500$ A m^{-1}, and the volume fraction 2 vol% (weight concentration $c_0 = 99$ g L^{-1}) is deduced from the specific magnetization of the nanoparticles, $m_{spe} = 2.75 \times 10^5$ A m^{-1} (55 emu/g in CGS units).

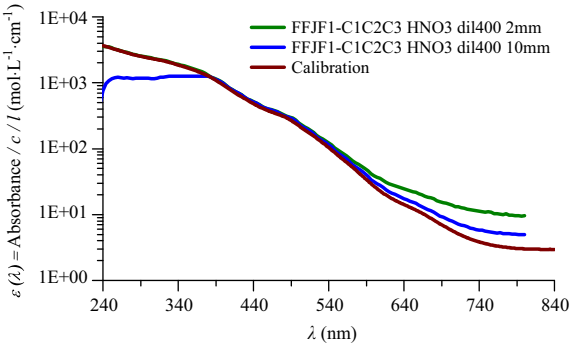

Fig. 2. Non-destructive determination of the iron oxide concentration by UV-vis spectroscopy. The spectrum of the sample diluted 400 times in HNO_3 at pH ~ 2 (for colloidal stability) is recorded between 240 and 800 nm. The extinction coefficient $\varepsilon(\lambda)$ calculated after normalization by the light path L (cm) and the equivalent iron concentration (1.24 mol L^{-1} as determined here) is fitted to a calibration curve obtained from measurements on samples at concentrations titrated by atomic emission spectroscopy [29]. Then the weight concentration $c_0 = 99$ g L^{-1} is simply deduced by multiplying 80 g mol^{-1} (~ half the molar mass of γ-Fe_2O_3). The deviation between the experimental spectra and the calibration curve towards large wavelengths is ascribed to a light scattering background (since the nanoparticles are particularly large in this study). The plateau for the larger light path (L = 10 mm) is an artifact due to the lower limit of the detector.

system tends to distort the AC hysteresis loops. In order to increase the maximum operational frequency, a spectral Fourier analysis of the signal is preformed in the calibration step (with no sample) to measure the distribution of non-desired harmonics. Next, the high frequency harmonic contribution is removed from each measurement. This is an essential point in order to get reliable measurements up to 1 MHz.

2.3. SAR measurements

The power volume density P_{vd} and *SAR* are obtained from the following equations:

$$P_{vd} = f \cdot \oint_T \mathbf{M_t} \cdot \mathbf{dH_t} \tag{3}$$

$$SAR = \frac{f}{c} \cdot \oint_T \mathbf{M_t} \cdot \mathbf{dH_t} \tag{4}$$

where $\mathbf{M_t}$ is the instantaneous magnetization (A m^{-1}) at time t, $\mathbf{H_t}$ the field intensity (A m^{-1}) at time t, f (Hz) the applied magnetic field frequency and c (kg m^{-3}) the nanoparticle weight concentration of iron oxide in the dispersing medium of volume V_d. In Eqs. (3) and (4), the units of P_{vd} and *SAR* values are given in W m^{-3} and W kg^{-1} respectively (although in this text, for convenience, W cm^{-3} and W g^{-1} are used). The integration is done over a period of the oscillating magnetic field, $T = 2\pi/f$.

To obtain the *SAR* values from the calorimetric method, Eq. (1) has been also used, for comparison. The specific heat capacity of water has been assumed to be 4.18 J g^{-1} K^{-1}. To obtain the initial temperature slope in Eq. (1), the temperature evolution curve has been fitted to a second order polynomial law [13], Eq. (5), and to an exponential relaxation law [19], Eq. (6). Here we aim at comparing both methods with two different measurement time intervals: T_{meas}=6 and 12 s (defined as the total duration of the applied magnetic field). In addition, the maximum derivative of temperature over time along the measurement period has been taken as initial slope of the curve, Eq. (7), too:

$$\Delta T = \left|\frac{dT}{dt}\right|_{t=0} \cdot t - at^2 \tag{5}$$

$$\Delta T = \tau \cdot \left|\frac{dT}{dt}\right|_{t=0} \cdot \left(1 - \exp\left(-\frac{t}{\tau}\right)\right) \tag{6}$$

$$\left|\frac{dT}{dt}\right|_{t=0} = \left(\frac{dT}{dt}\right)_{max} \quad (7)$$

3. Result and discussions

Fig. 4 shows the dynamic hysteresis cycles of the maghemite nanoparticles sample at applied magnetic field frequencies of 394 and 785 kHz as well as the *SAR* values obtained from the integration of their area according to Eq. (4). The dependence of *SAR* with the applied magnetic field intensity, H_{app}, is almost quadratic below 10 kA m^{-1}, while above this value, it is almost linear. The *SAR* values at 394 kHz are in good agreement with values measured by calorimetry on similar large size-sorted maghemite nanoparticles [17] 72 W/g (compared to 70.4 W/g here) under a field of 11 kA m^{-1} and 200 W/g (vs. 193 W/g here) under a field of 24 kA m^{-1}. In the same reference, the *SAR* values were estimated from AC susceptometry: the corresponding values were 70 W/g and 215 W/g for field values of 11 and 24 kA m^{-1} respectively. The deviation between calorimetry and AC susceptometry for the larger field value in this previous work [17] is likely ascribed to the use of Eq. (4) in a linearized form (with some correction factor), introducing the susceptibility $\chi'' = \mathbf{M_t}/\mathbf{H_t}$. Here we compute the whole integral on a field period T without simplification, therefore our setup can be named "AC magnetometer" rather than "AC susceptometer".

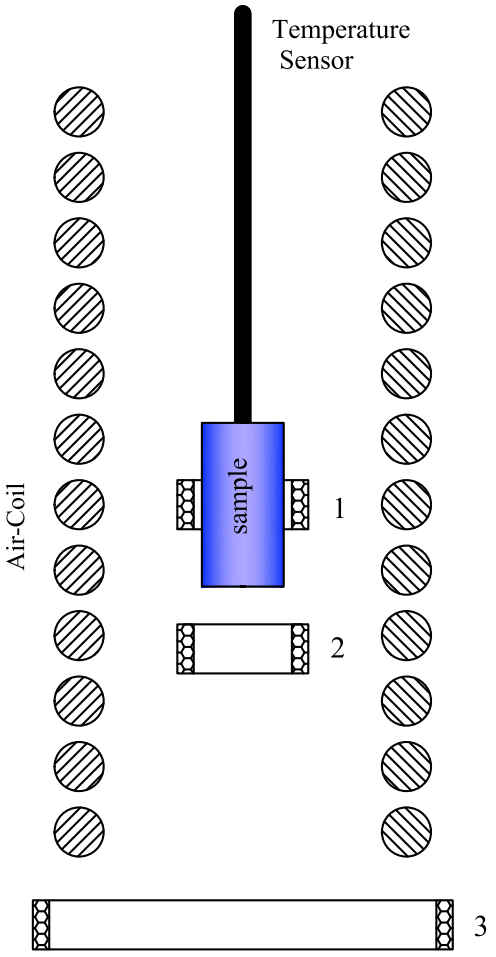

Fig. 3. Schematic of the experimental setup.

3.1. SAR measurement

For applied magnetic field frequencies of 70, 394, 785, 958 kHz and intensities of 11 and 24 kA m^{-1}, *SAR* has been measured by both calorimetry and AC magnetometry. To obtain the initial time slope in Eq. (1), the three different procedures described in the previous section are used. Table 1 and Fig. 5 compare the so-obtained *SAR* values. In order to distinguish between the *SAR* values obtained from different methods, SAR_{area} represents the values obtained from hysteresis loop area. SAR_{2poly} has been obtained fitting the temperature evolution curve to the second order polynomial of Eq. (5), whereas SAR_{expo} has been obtained by fitting to the exponential of Eq. (6), with time intervals of 6 and 12 s. Finally, SAR_{DTmax} is obtained by the maximum temperature derivative over time, Eq. (7), along measurement time.

As it can be observed in Table 1 and Fig. 5, when P_{vd} is above 1 W cm^{-3}, the *SAR* values obtained by thermal and electromagnetic methods differ by less than 12%. However, *SAR* values obtained by calorimetric methods depend on the procedure used to obtain the initial time slope in Eq. (1). When temperature evolution is fitted to a second order polynomial with a time interval of 12 s, values obtained from both calorimetry and AC magnetometry differ the less (below 6%). When the temperature measurement time interval is 6 s, however, the obtained SAR_{2poly} and SAR_{expo} values are smaller than SAR_{area}. On the other hand, when the maximum time derivative is taken SAR_{DTmax} values are larger.

Fig. 6 represents the temperature evolution of the sample after the magnetic field is switched on for different measured P_{vd}. As it can be observed, when P_{vd} is 5.38 and 6.8 W cm^{-3}, the temperature initially rises slowly and after 0.5 s, it starts to increase rapidly. Similar behaviour can be found in Wang et al. [13] but 5 s after the field is applied. Therefore, when a small temperature measurement time interval is considered, the obtained initial

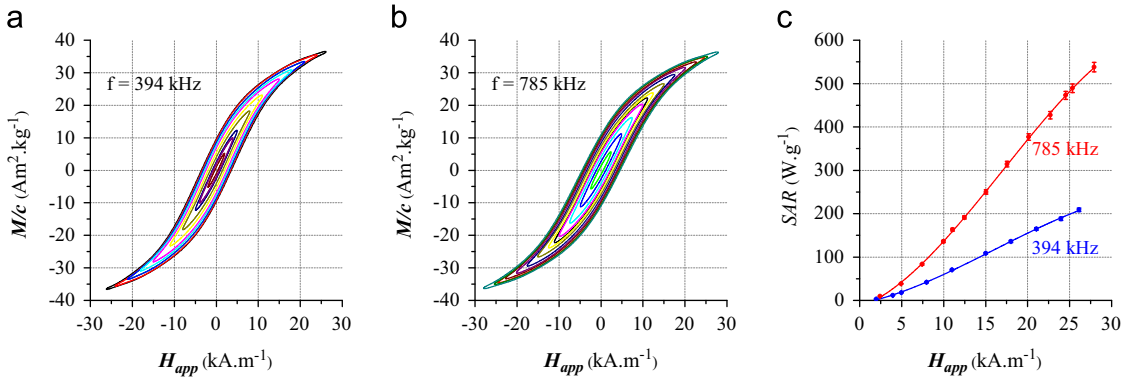

Fig. 4. Hysteresis cycles of maghemite nanoparticles (a) at 394 kHz, (b) at 785 kHz. (c) *SAR* values obtained from the area of the cycles, versus applied magnetic field at 394 and 785 kHz. Sample volume is $V_d = 1.5$ mL and maghemite concentration $c = 33$ g L^{-1}.

Table 1
Measured *SAR* values with AC magnetometry (SAR_{area}) and calorimetric methods, see text.

H_{app} (kA m^{-1})	*Freq.* (kHz)	AC magnetometry		Calorimetric method. $SAR_{thermal}$ (W g^{-1})				
		P_{vd} (W cm^{-3})	SAR_{area} (W g^{-1})	SAR_{2poly}		SAR_{expo}		SAR_{DTmax}
				6 s	12 s	6 s	12 s	
11	75	0.22 ± 0.01	8.3 ± 0.2	13 ± 1	10.3 ± 0.5	15 ± 2	10.8 ± 0.6	10 ± 1
11	394	1.91 ± 0.02	70.4 ± 0.7	67 ± 1	70.6 ± 0.5	67 ± 1	70.8 ± 0.5	77 ± 1
11	785	4.41 ± 0.05	163 ± 2	157 ± 1	171 ± 1	157 ± 1	172 ± 1	178 ± 1
11	958	5.6 ± 0.2	207 ± 4	193 ± 2	209 ± 1	193 ± 1	210 ± 1	217 ± 1
24	394	5.27 ± 0.07	193 ± 2	186 ± 2	192 ± 1	185 ± 2	193 ± 1	202 ± 1
24	785	12.8 ± 0.2	472 ± 5	442 ± 6	474 ± 2	442 ± 6	478 ± 2	502 ± 1
24	958	16.1 ± 0.2	595 ± 5	570 ± 6	629 ± 2	570 ± 6	640 ± 2	667 ± 1

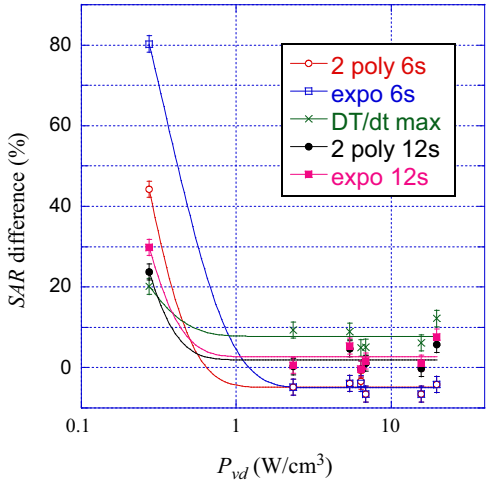

Fig. 5. Relative difference between the *SAR* values obtained from calorimetric methods and AC magnetometry as a function of power volume density P_{vd} (logarithmic scale).

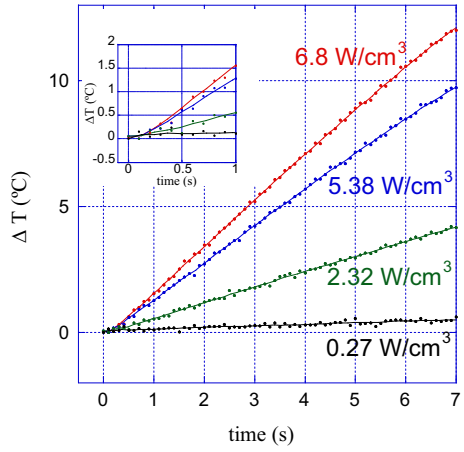

Fig. 6. Sample's temperature increase evolution with time for different measured P_{vd}. The inset displays the non-linearities of temperature evolution during the first second.

temperature slope in Eq. (1) can be underestimated due to this phenomenon that can be ascribed to thermal inertia of the measuring system.

When P_{vd} is below 1 W cm^{-3}, however, the difference between both methods increases up to 80% (see Fig. 5). In this case, however, calorimetric methods are less accurate due to the heat flux coming out the sample holder. As it can be observed in Fig. 6, the temperature increase is very small when P_{vd} is 0.27 W cm^{-3}. Moreover, fitting the temperature evolution curve to the exponential in Eq. (6) gives a total power of 0.13 W flowing out of the sample when ΔT is 1 °C. This outgoing power is comparable with the total power generated by the sample (0.4 W), corresponding to the plateau temperature reached when the created and lost power compensate.

4. Conclusions

This paper presents an AC magnetometer built to measure dynamic hysteresis cycles of magnetic nanoparticle dispersions, which extends the range of measurement from 50 kHz to 1 MHz, giving valuable information on their dynamic magnetic behaviour. By means of this device, the *SAR* of quasi-spherical maghemite nanoparticles with a distribution of the magnetic core sizes around 12 nm in size has been measured by integrating the area of the AC hysteresis loop. The obtained values are comparable to previously measured values in maghemite nanoparticles with similar characteristics (synthesis route and distribution of sizes).

To check the method, the *SAR* of the same sample has been measured also by calorimetric methods. In general, the values obtained by both types of methods are similar within an error of 12%. However the values obtained by calorimetry depend on the curve fitting procedure to obtain the initial time slope in Eq. (1). The uncertainties arise from non-linearity in the initial temperature evolution curve (see Fig. 6). On the other hand, when the dissipated power density P_{vd} is too small (be it from a not optimal frequency or a too low concentration) the non-adiabatic behaviour of the sample holder increases the differences between calorimetric methods.

Due to a smaller measurement uncertainty, AC magnetometry results in a more accurate and direct method to measure *SAR* values of nanoparticle dispersions than calorimetric methods. This advantage is true for applied magnetic field frequencies from 50 kHz to 1 MHz and intensities up to 24 kA m^{-1}. Moreover, the time required in the measurement process is shorter because a previous thermalization is not required.

References

[1] J. Dickson, Hyperthermia in the treatment of cancer, Lancet 1 (1979) 202–205.
[2] H.R. Moyer, K.A. Delman, The role of hyperthermia in optimizing tumor response to regional therapy, Int. J. Hyperth. 24 (2008) 251–261.
[3] M. Palazzi, S. Maluta, S. Dall'Oglio, M. Romano, The role of hyperthermia in the battle against cancer, Tumori 96 (2010) 902–910.
[4] R.W.Y. Habash, B.M. Ali, M.K. Abdullah, K.B. Seman, M.D. Baba, M. Esa, Performance analysis of a multicast system in WDM single-hop broadcast-and-select optical network, in: 2006 International RF and Microwave Conference, Proceedings, 2006, pp. 448–454.
[5] A. Jordan, R. Scholz, P. Wust, H. Fahling, R. Felix, Magnetic fluid hyperthermia (MFH): cancer treatment with ac magnetic field induced excitation of biocompatible superparamagnetic nanoparticles, J. Magn. Magn. Mater. 201 (1999) 413–419 8th International Conference on Magnetic Fluids (ICMF), Timisoara, Romania, June 29–July 03, 1998.

Please cite this article as: E. Garaio, et al., Journal of Magnetism and Magnetic Materials (2013), http://dx.doi.org/10.1016/j.jmmm.2013.11.021

[6] B. Quesson, M. Merle, M.O. Kohler, C. Mougenot, S. Roujol, B.D. de Senneville, C.T. Moonen, A method for MRI guidance of intercostal high intensity focused ultrasound ablation in the liver, Med. Phys. 37 (2010) 2533–2540.
[7] K. Maier-Hauff, F. Ulrich, D. Nestler, H. Niehoff, P. Wust, B. Thiesen, H. Orawa, V. Budach, A. Jordan, Efficacy and safety of intratumoral thermotherapy using magnetic iron-oxide nanoparticles combined with external beam radiotherapy on patients with recurrent glioblastoma multiforme, J. Neuro-Oncol. 103 (2011) 317–324.
[8] R. Hergt, S. Dutz, R. Mueller, M. Zeisberger, Magnetic particle hyperthermia: nanoparticle magnetism and materials development for cancer therapy, J. Phys. Condens. Matter 18 (2006) S2919–S2934.
[9] R.E. Rosenweig, Heating magnetic fluid with alternating magnetic field, J. Magn. Magn. Mater. 252 (2002) 370.
[10] M. Ma, Y. Wu, J. Zhou, Y. Sun, Y. Zhang, N. Gu, Size dependence of specific power absorption of Fe_3O_4 particles in ac magnetic field, J. Magn. Magn. Mater. 268 (2004) 33–39.
[11] J.-P. Fortin, C. Wilhelm, J. Servais, C. Menager, J.-C. Bacri, F. Gazeau, Size-sorted anionic iron oxide nanomagnets as colloidal mediators for magnetic hyperthermia, J. Am. Chem. Soc. 129 (2007) 2628–2635.
[12] E. Kita, S. Hashimoto, T. Kayano, M. Minagawa, H. Yanagihara, M. Kishimoto, K. Yamada, T. Oda, N. Ohkohchi, T. Takagi, T. Kanamori, Y. Ikehata, I. Nagano, Heating characteristics of ferromagnetic iron oxide nanoparticles for magnetic hyperthermia, J. Appl. Phys. 107 (2010) 11th Joint MMM-Intermag Conference, Washington, DC, January 18–22, 2010.
[13] S.-Y. Wang, S. Huang, D.-A. Borca-Tasciuc, Potential sources of errors in measuring and evaluating the specific loss power of magnetic nanoparticles in an alternating magnetic field, IEEE Trans. Magn. 49 (2013) 255–262.
[14] S. Huang, S.-Y. Wang, A. Gupta, D.-A. Borca-Tasciuc, S.J. Salon, On the measurement technique for specific absorption rate of nanoparticles in an alternating electromagnetic field, Meas. Sci. Technol. 23 (2012).
[15] E. Natividad, M. Castro, A. Mediano, Adiabatic vs. non-adiabatic determination of specific absorption rate of ferrofluids, J. Magn. Magn. Mater. 321 (2009) 1497–1500.
[16] D. Habault, A. Dery, J. Leng, S. Lecommandoux, J.-F.L. Meins, O. Sandre, Droplet microfluidics to prepare magnetic polymer vesicles and to confine the heat in magnetic hyperthermia, IEEE Trans. Magn. 49 (2013) 182–190.
[17] F. Ahrentorp, A.P. Astalan, C. Jonasson, J. Blomgren, B. Qi, O.T. Mefford, M. Yan, J. Courtois, J.-F. Berret, J. Fresnais, O. Sandre, S. Dutz, R. Mueller, C. Johansson, Sensitive high frequency ac susceptometry in magnetic nanoparticle applications, AIP Conf. Proc. 1311 (2010) 213–223, 8th International Conference on the Scientific and Clinical Applications of Magnetic Carriers, Rostock, Germany, May 25–29, 2010.
[18] P. Cobos, M. Maicas, M. Sanz, C. Aroca, High resolution system for nanoparticles hyperthermia efficiency evaluation, IEEE Trans. Magn. 47 (2011) 2360–2363, Conference on International Magnetics (INTERMAG), Taipei, Taiwan, April 25–29, 2011.
[19] M. Bekovic, A. Hamler, Determination of the heating effect of magnetic fluid in alternating magnetic field, IEEE Trans. Magn. 46 (2010) 552–555 19th International Conference on Soft Magnetic Materials, Turin, Italy, September 06–09, 2009.
[20] M. Veverka, P. Veverka, O. Kaman, A. Lancok, K. Zaveta, E. Pollert, K. Knizek, J. Bohacek, M. Benes, P. Kaspar, E. Duguet, S. Vasseur, Magnetic heating by cobalt ferrite nanoparticles, Nanotechnology 18 (2007).
[21] B. Mehdaoui, J. Carrey, M. Stadler, A. Cornejo, C. Nayral, F. Delpech, B. Chaudret, M. Respaud, Influence of a transverse static magnetic field on the magnetic hyperthermia properties and high-frequency hysteresis loops of ferromagnetic FeCo nanoparticles, Appl. Phys. Lett. 100 (2012).
[22] S.A. Gudoshnikov, B.Y. Liubimov, N.A. Usov, Hysteresis losses in a dense superparamagnetic nanoparticle assembly, AIP Adv. 2 (2012).
[23] S.A. Gudoshnikov, B.Y. Liubimov, Y.S. Sitnov, V.S. Skomarovsky, N.A. Usov, Ac magnetic technique to measure specific absorption rate of magnetic nanoparticles, J. Supercond. Nover Magn. 26 (2013) 857–860 3rd International Conference on Superconductivity and Magnetism (ICSM), Istanbul, Turkey, April 29–May 04, 2012.
[24] R. MASSART, Preparation of aqueous magnetic liquids in alkaline and acidic media, IEEE Trans. Magn. 17 (1981) 1247–1248.
[25] F. Tourinho, R. Franck, R. Massart, R. Perzynski, Synthesis and magnetic properties of manganese and cobalt ferrite ferrofluids, Prog. Colloid Polym. Sci. 79 (1989) 128–134.
[26] R. Massart, E. Dubois, V. Cabuil, E. Hasmonay, Preparation and properties of monodisperse magnetic fluids, J. Magn. Magn. Mater. 149 (1995) 1–5.
[27] P. Arosio, J. Thevenot, T. Orlando, F. Orsini, M. Corti, M. Mariani, L. Bordonali, C. Innocenti, C. Sangregorio, H. Oliveira, S. Lecommandoux, A. Lascialfari, O. Sandre, Hybrid iron oxide-copolymer micelles and vesicles as contrast agents for MRI: impact of the nanostructure on the relaxometric properties, J. Mater. Chem. B 1 (2013) 5317–5328.
[28] Q. Vuong, J. Berret, J. Fresnais, Y. Gossuin, O. Sandre, A universal scaling law to predict the efficiency of magnetic nanoparticles as MRI T2-contrast agents, Adv. Healthcare Mater. 4 (2012).
[29] A. Galimard, M. Safi, N. Ould-Moussa, D. Montero, H. Conjeaud, J. Berret, Thirty-femtogram detection of iron in mammalian cells, Small 8 (13) (2012) 2036–2044.
[30] F. Plazaola, E. Garaio, J.M. Collantes, I. Castellanos, M. Insausti, I.G. de Muro, J.A. Garcia, Specific absorption rate of magnetite nanoparticle powders with and without surrounding organic ligands, J. Nanosci. Nanotechnol. 12 (2012) 7451–7455.

Please cite this article as: E. Garaio, et al., Journal of Magnetism and Magnetic Materials (2013), http://dx.doi.org/10.1016/j.jmmm.2013.11.021